ACADEMIC PRESS

Available online at www.sciencedirect.com

SCIENCE DIRECT®

Journal of Magnetic Resonance 158 (2002) 79–85

JMR Journal of Magnetic Resonance

www.academicpress.com

In vivo magnetic resonance microscopy of brain structure in unanesthetized flies☆

Alan Jasanoff[a,*] and Phillip Z. Sun[a,b,c]

[a] *Whitehead Institute for Biomedical Research, Nine Cambridge Center, Cambridge, MA 02142, USA*

[b] *Department of Nuclear Engineering, Massachusetts Institute of Technology, 150 Albany Street, Cambridge, MA 02139, USA*

[c] *Harvard–MIT, Division of Health Sciences and Technology, Radiological Science and Technology Joint Program, 77 Massachusetts Avenue, E25-519, Cambridge, MA 02139, USA*

Received 7 March 2002; revised 28 June 2002

Abstract

We present near-cellular-resolution magnetic resonance (MR) images of an unanesthetized animal, the blowfly *Sarcophaga bullata*. Immobilized flies were inserted into a home-built gradient probe in a 14.1-T magnet, and images of voxel size $(20–40\,\mu m)^3$—comparable to the diameter of many neuronal cell bodies in the fly's brain—were obtained in several hours. Use of applied field gradients on the order of 60 G/cm allowed minimally distorted images to be produced, despite significant susceptibility differences across the specimen. The images we obtained have exceptional contrast-to-noise levels; comparison with histology-based anatomical information shows that the MR microscopy faithfully represents patterns of nervous tissue and allows distinct brain regions to be clearly identified. Even at the highest resolutions we explored, morphological detail was pronounced in the apparent absence of instabilities or movement-related artifacts frequently observed during imaging of live animal specimens. This work demonstrates that the challenges of noninvasive in vivo MR microscopy can be overcome in a system amenable to studies of brain structure and physiology.

1. Introduction

Unlike other approaches to studying animal physiology in vivo, magnetic resonance imaging (MRI) can at the same time operate at a resolution of several micrometers and detect signals from entire intact three-dimensional (3D) specimens [1,2]. Through the combined use of high-field magnets and NMR probes optimized for microimaging, several research groups have managed to combat limitations of MRI in order to generate reasonably detailed images of biological samples at or near cellular resolution [3–6]. The first MRI images of a single cell, an isolated ovum of *Xenopus laevis* about 1 mm in diameter, were reported over a decade ago [7]. They have been followed by more recent studies of somewhat smaller cells such as detached invertebrate neurons and unicellular algae [4,8], and also of microscopic structure in multicellular plants [9,10]. Observation of cellular organization in animals is complicated by the fact that adjacent cells of a given tissue type usually have similar proton content and relaxation parameters and are thus difficult to distinguish based on MRI contrast differences. In some cases it has been possible to study individual cells in animals by cell-specific targeting or injecting paramagnetic chemicals (contrast agents) which alter the local MRI intensities [11–14]. There is currently a great deal of interest in the development of novel contrast agents with tailored in vivo localization or physiological sensitivity, as well as in the introduction of flow and diffusion-based imaging techniques for the analysis of microscopic tissue structure and plasticity [15].

As the reach of biological MR microscopy expands, it becomes desirable to explore animal models which are particularly suited to in vivo testing and application of new pulse sequences and contrast agents. To this end, we have chosen to work with blowflies (large flies of the

☆ *Abbreviations:* MR, magnetic resonance; MRI, magnetic resonance imaging; 3D, three dimensional; voxel, volume element; RF, radiofrequency; TE, echo time; TR, recycle time; FOV, field of view.

* Corresponding author. Fax: 617-258-0376.
E-mail address: jasanoff@wi.mit.edu (A. Jasanoff).

1090-7807/02/$ - see front matter © 2002 Elsevier Science (USA). All rights reserved.
PII: S1090-7807(02)00063-0

genera *Sarcophaga* and *Calliphora*). These insects are easy to immobilize and maintain intact and awake, and have been used in the past for a wide range of electrophysiological and optical imaging experiments [16]. Like many invertebrates, they have small brains containing relatively large neurons, some on the order of 30 μm in diameter [17,18]. The flies also lack hemoglobin or a hemodynamic response to brain stimulation, making them ideal for testing new physiology-dependent contrast mechanisms. Blowflies are roughly 5 mm wide, making them small enough to be imaged in today's highest field commercial magnets. In this paper, we demonstrate that a home-built imaging probe operating at 14.1 T can produce exceptionally clear high-resolution images of live unanesthetized blowflies. The images provide a detailed view of internal anatomy; cross sections of a $(19.5\,\mu m)^3$-voxel image allow identification of major brain regions and nerves, and correlate closely with histology. Motion artifacts are absent, and the system has signal-to-noise and stability suitable for future high-resolution studies.

2. Methods

2.1. Sample preparation

Adult female *Sarcophaga bullata* were obtained as pupae (Carolina Biol. Supply) and imaged from 1 to 3 weeks after eclosion. Specimens were generally 10–12 mm in length and 70–110 mg in weight. Flies were temporarily anesthetized with CO_2, immobilized by applying wax to wings and joints, and inserted into 5-mm inner diameter plastic tubes. In some experiments the fly's proboscis was either removed or fixed to the head with wax. Flies quickly recovered from CO_2 after the mounting procedure and were imaged without further anesthesia. Mounted blowflies typically survived at least one day without further feeding, or several days if fed.

2.2. Imaging hardware

Imaging experiments were performed using a home-built imaging probe inserted into a 14.1-T (600 MHz) Bruker AMX II spectrometer. Gradient coils built into the probe were based on earlier designs [3,4,6]. Phantom images (not shown) demonstrated linearity of the gradients over a roughly $(5\,mm)^3$ cube, in agreement with calculations from a priori modeling. A Helmholtz-like radiofrequency coil (Fig. 1, inset), designed to fit around the head of a blowfly, was wrapped around a polyimide former and inserted from one end of a horizontal aperture in the probe's gradient set. A fly specimen prepared as described above was inserted in its holder from the other end of the gradient set aperture. In the probe's fully assembled configuration, the RF coil was centered with respect to the gradient coils, and the fly's head was approximately centered under the RF coil.

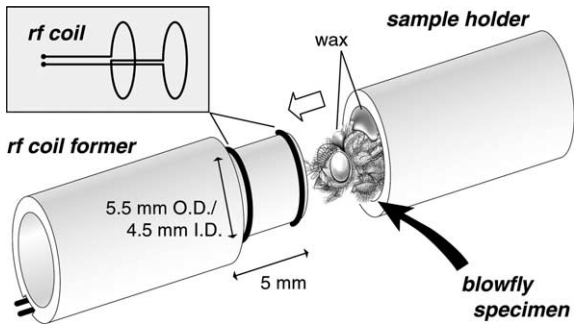

Fig. 1. Experimental setup for in vivo imaging. A live blowfly (*S. bullata*) is immobilized and fixed with wax into a plastic tube. The specimen is inserted from one end of an aperture into the imaging probe's gradient set, while the radiofrequency coil (inset), wrapped over a polyimide former, is inserted from the opposite end, so that the coil sits directly over the fly's head. The fly picture was adapted from [26]. The gradient set and RF coil are part of a custom-built probe designed for MRI microscopy in a Bruker 14.1 T system.

2.3. Data acquisition

The images described here were acquired at 25 °C using spin-echo pulse sequences with echo times (TE) of 3–12 ms, relaxation delays (TR) of 250–500 ms, and maximum gradient strengths of 60 G/cm. In all 3D images, standard spin-warp methods were used for rectilinear grid sampling of k-space. Slice selection was performed with an initial $\pi/2$ spatially selective excitation pulse. On a routine basis, stability of the experimental setup was verified by comparing identically acquired two-dimensional images measured before and after long acquisition periods, and by visual inspection of the specimen to ensure that it had remained alive throughout the experiment. Fields of view (FOVs) and further details of specific experiments are given below in the text and figure captions.

2.4. Data processing and display

Complex k-space data were processed with squared-sinebell apodization and Fourier transformed to real space magnitudes using the program Matlab (Mathworks). Voxel resolutions we report are those determined solely by the acquisition parameters. No zero-filling, resolution enhancement, or additional filtering was performed, with the exception of the imaging of Fig. 4, which was digitally rotated (with bicubic resampling) for optimal viewing. Analysis of resolution, signal-to-noise, and stability were performed using Matlab (see Results & Discussion). Signal to noise was determined by comparing mean signal (mean of all voxels over two standard deviations from the noise) to the noise standard deviation

(calculated from the width of a Gaussian fit to the low-intensity maximum of an image's intensity histogram). Three-dimensional visualization was accomplished with Imaris (Bitplane AG) and Voxelview (Vital Images). Figures were generated with Adobe Illustrator and Adobe Photoshop.

3. Results and discussion

3.1. Imaging of live blowflies at 14.1 T

A practical challenge to 3D imaging a live fly at 20-μm resolution by MRI is the need to keep the animal fixed for the required data acquisition times from many minutes to hours. Previous MRI studies of insects have achieved roughly comparable resolution, but used dead or developing specimens which could not move on the timescale of the imaging experiment [19–21]. The blowflies we used are relatively easy to immobilize (Methods and Fig. 1), and similar blowfly preparations have been used extensively in electrophysiological and optical imaging studies (reviewed in [16]). The general success of this procedure could be verified by eye or under a microscope, where surgically exposed neurons individually injected with fluorescent dyes were observed to remain in place over time (data not shown).

A technical challenge to MR imaging of animals in a 14.1 T instrument is the presence of large magnetic susceptibility differences at tissue boundaries and air/tissue interfaces [22]. This macroscopic susceptibility inhomogeneity results in spatially varying magnetic fields and local field gradients—effects which are emphasized at high field and potentially introduce major distortions in the frequency-encoding dimension of a spin-warp image. Fig. 2 shows a series of cross sections through images of the same live blowfly's head, acquired with three different frequency-encoding gradient strengths: 15, 30, and 59 G/cm. The image acquired with the strongest gradient strength requires the full acquisition bandwidth available (125 kHz) on the imaging spectrometer we used, but shows good symmetry and little obvious distortion. By contrast, the image taken at a gradient strength of 15 G/cm is severely distorted; comparable anatomical regions are up to 6 voxels (out of 128, for a 5-mm FOV) displaced from their locations in the 59 G/cm image, indicating that susceptibility inhomogeneity across the field of view is on the order of 2.5 parts per million. These data demonstrate a requirement to use gradient strengths well over 50 G/cm for distortionless imaging of blowflies at 14.1 T.

3.2. Tissue morphology and brain structure

Images of unanesthetized blowflies representing the level of anatomical detail obtained with our setup are presented in Figs. 3 and 4. Fig. 3 shows front, side, and top views of a $(39\,\mu m)^3$-voxel size 3D MR image of a blowfly's head and anterior thorax (acquisition time 6 h), as well as a conventional photograph of a blowfly for comparison. The MR image was acquired with a recycle time (TR) of 300 ms and an echo time (TE) of 3 ms, and contrast in the image therefore reflects primarily T_1 relaxation-related differences as well as variations in proton content. Truncation of the image at the thorax reflects falloff of the RF field. Anatomical structures which are either solid-phase or low in water content are clearly invisible in the MR image—among them the chitinous exoskeleton of the fly, the gas-filled tracheae and air sacs of the fly's respiratory system, and the wax used in specimen preparation. The images do show pronounced signal for neural tissue. The brain and optic lobes occupy much of the fly's head capsule and account for the bent dumbbell shape on the left-hand

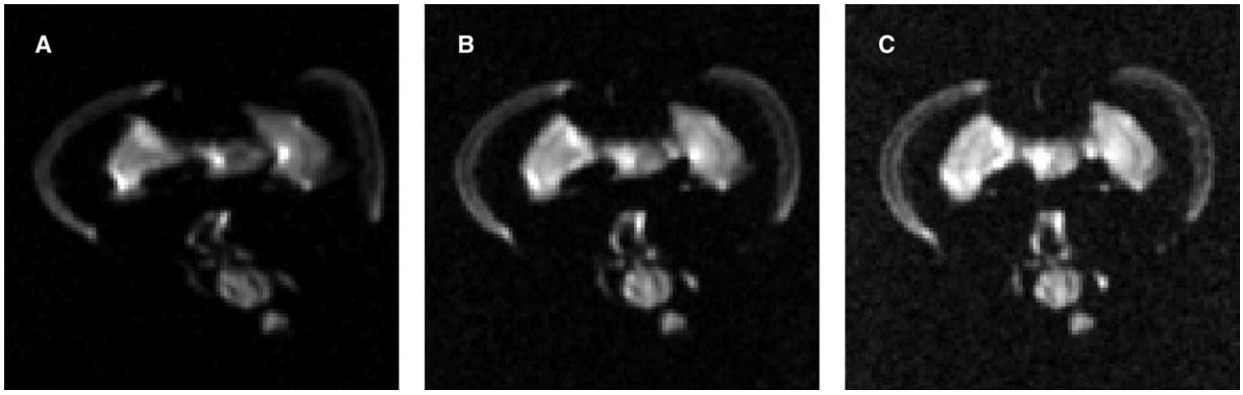

Fig. 2. Cross sections through the head of a blowfly imaged with three gradient strengths in the frequency-encoding dimension (horizontal on the page): (A) 15 G/cm, (B) 30 G/cm, and (C) 59 G/cm. The obvious warping of the image in panel A, particularly in the frequency-encoding direction (compared with panel C), indicates the severity of susceptibility effects in images of the animal at 14.1 T. The image taken with highest gradient strength shows essentially no distortion, however, and indicates that susceptibility effects can be overcome with the use of modest gradients and some sacrifice in bandwidth. Other acquisition parameters: TR = 250 ms, TE = 3 ms, 2 signal averages per echo, FOV $5 \times 5 \times 2.5$ mm, $128 \times 128 \times 64$ data size, total experimental time 1.5 h.

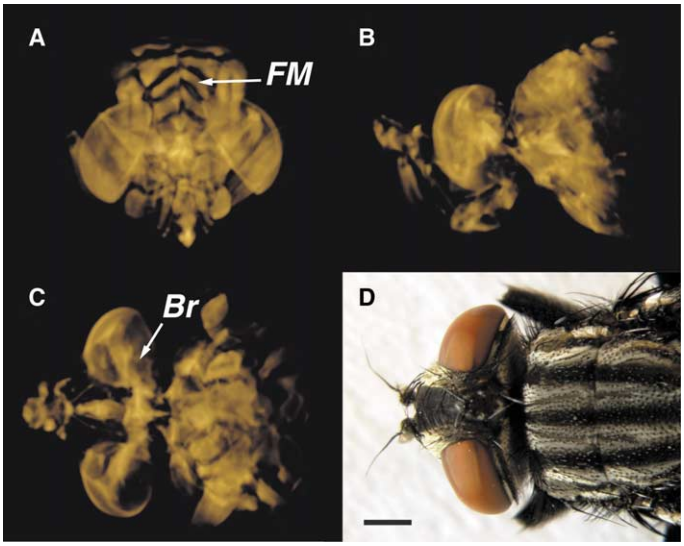

Fig. 3. MRI images with voxel size of $(39\,\mu m)^3$, showing the head and anterior thorax of a live blowfly. The 3D image data set is rendered as a semitransparent volume, viewed in projection from the (A) front, (B) side, and (C) top. Panel D shows a photograph of another blowfly, viewed from the top, for comparison (scalebar = 1 mm). The MRI data were acquired using a T_1-weighted spin echo pulse sequence on a 14.1-T microscope. The entire fly (~12 mm long) was imaged without slice selection; truncation of the image at the thorax reflects falloff of the RF field. Many anatomical features are clearly distinguishable, especially the musculature and nervous tissue. The fly's flight muscles (FM) are labeled in panel A, and the brain (Br) is labeled in panel C. The blowfly's dark striped exoskeleton, seen in panel D, is invisible to MRI and does not appear in panels A–C. The protruding structure at the leftmost extremes of panels B and C is the ptilinum of this fly (not present in the fly of panel D). Acquisition parameters: TR = 300 ms, TE = 3 ms, four signal averages per echo, FOV $10 \times 5 \times 5$ mm, $256 \times 128 \times 128$ data size, total experimental time 6 h.

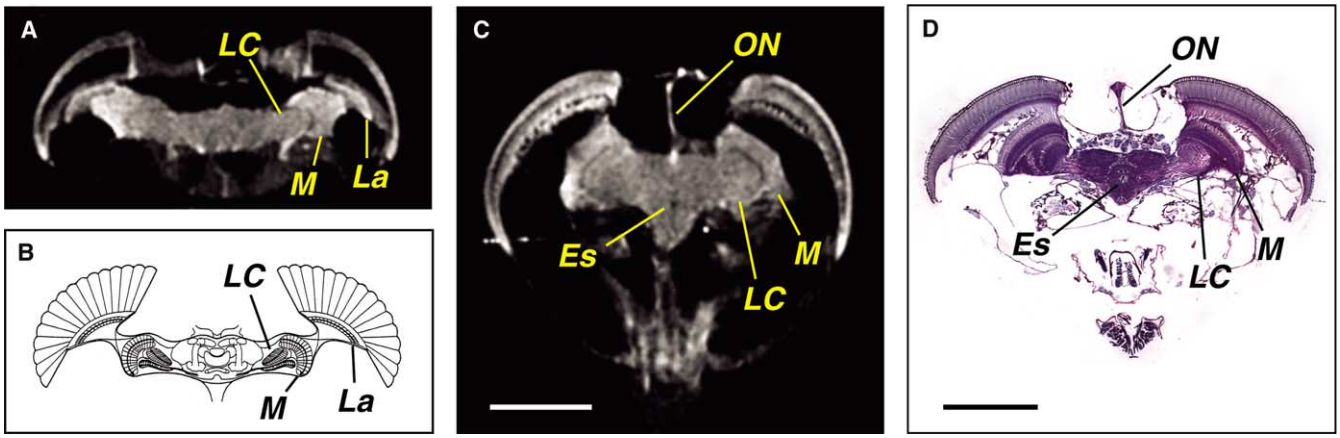

Fig. 4. Demonstration of the detail of brain structure revealed in MRI images of the blowfly brain taken with a voxel size of $(19.5\,\mu m)^3$. Panel (A) shows an anatomically horizontal cross section through an image of a living blowfly's head, acquired with slice selection and a voxel size $(19.5\,\mu m)^3$, showing boundaries between three major brain regions responsible for visual processing: the lamina (La), medulla (M), and lobula complex (LC). Panel (B) is a schematic drawing of blowfly brain anatomy, provided for comparison with (A) and labeled similarly (adapted from [23]). Panel (C) is a coronal cross section through the same blowfly image as in (A), illustrating again the boundary between the medulla and lobula complex, as well as finer features of neuroanatomy such as the ocellar nerve (ON) which connects the fly's accessory "simple" eyes to the brain, and a cross section of the esophagus (Es), which runs through the brain. These structures are all present and labeled in panel (D), which is a corresponding silver-stained 5-μm section from a different blowfly (courtesy Z. Schoening). Acquisition parameters for the MRI image (panels A & C): TR = 500 ms, TE = 3 ms, four transients per echo, FOV $5 \times 5 \times 2.5$ mm, $256 \times 256 \times 128$ data size, experimental time 19 h. Scalebars = 1 mm.

side of Fig. 3C (labeled Br). Musculature also has a high water content and produces strong signal in these images; the most striking example is the mosaic-like array of flight muscles in the thorax (labeled FM, Fig. 3A). MRI intensity from fatty tissue is not as pronounced in the 14.1 T images as it is in images taken at lower field, but adipocytes and fatty deposits can be identified based on their relative T_2 and diffusional properties (Sun et al., in preparation).

Higher-resolution images demonstrate the ability of 14.1-T MRI experiments to produce maps of brain structure in the living fly. Fig. 4A presents a horizontal

cross section through a $(19.5\,\mu m)^3$-voxel 3D image of a blowfly's head, obtained with 500 ms TR and 3 ms TE (acquisition time 18 h). The three major visual ganglia (lamina, medulla, and lobula complex) are easily identifiable in the image, and an anatomical drawing is provided for comparison (Fig. 4B; [23]). In the MR cross section, the fly's compound eyes each appear as two high-intensity arcs sandwiching a dark interior. The more lateral arc is approximately 60 μm thick and probably corresponds to corneae and cone cells of the ommatidia, while the medial or inner arcs correspond to the ganglion cell layer of each eye. The inner layer of the fly's eye is an array of lipid-rich oriented microvilli [24]; it is likely that these regions have long T_1 and short T_2 relaxation rates and therefore do not contribute strong MRI intensity, even when short echo times are used. Major divisions of the brain are also apparent in the coronal section of Fig. 4C, as well finer features of the fly's neuroanatomy such as the ocellar nerve (labeled ON), which connects the central brain to three "simple eyes" at the top of the head, and a cross section of the esophagus (Es), which passes through a stoma in the middle of the brain [25]. These specific features are depicted in a silver-stained coronal section of another blowfly's brain (Fig. 4D). Comparison of the MR and conventional microscopy images indicates that brain morphology down to the level of structures as small as 30–50 μm in diameter are well represented by MRI.

3.3. Resolution, signal-to-noise, and stability

MRI studies of physiology and structure using the live blowfly preparation we have developed will be limited by the resolution, signal-to-noise, and stability achievable with the imaging system. Resolution of the blowfly microscopy is indicated in part by the minimum size of features which appear in the images. For instance, the esophagal cross section and the ocellar nerve labeled in Fig. 4 are both structures of diameter 30 to 50 μm (about two voxels) whose measurements correspond well with dimensions taken from fixed and sectioned tissue. Some large cells in the blowfly's brain have dimensions on the order of the voxel size of $(19.5\,\mu m)^3$, but presumably because individual cells in homogeneous tissue have contrast properties similar to those of their neighbors, they do not stand out in this preparation. Boundaries and interstitial spaces between neurons in the fly brain are likewise indiscernible in these images, and much higher resolution (probably 1–2 μm) would be required to resolve them.

The average signal-to-noise ratio (SNR) of the blowfly images was estimated using intensity histograms derived from the MRI data (Methods and Fig. 5A). For

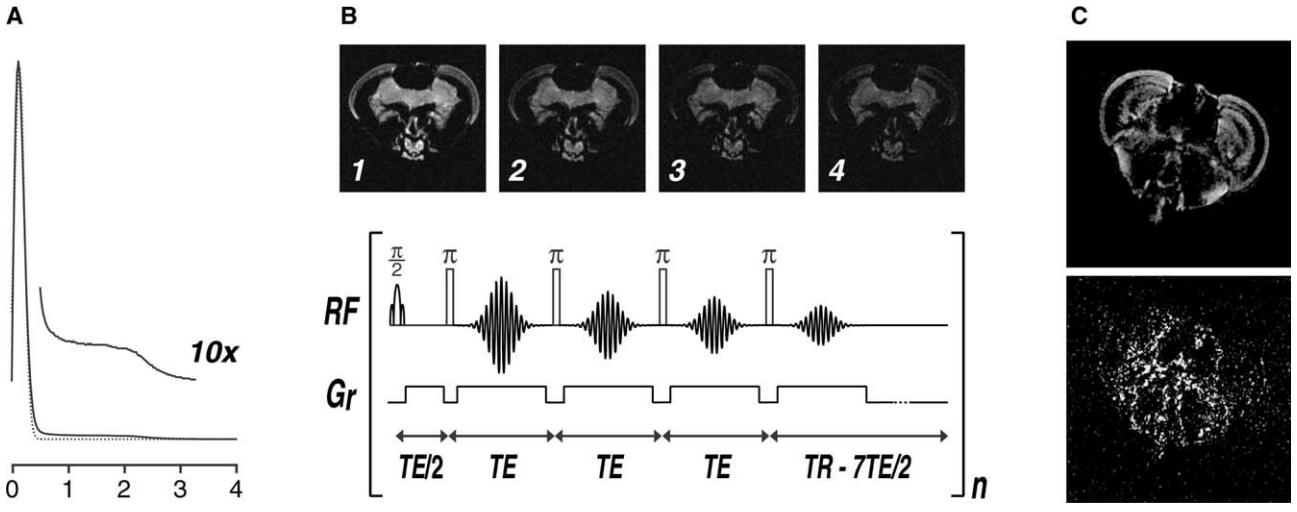

Fig. 5. SNR and stability of the in vivo imaging system. (A) Intensity histogram from a $(19.5\,\mu m)^3$-voxel image (horizontal scale in arbitrary intensity units). The major peak corresponds to voxels with little or no intensity and can be fit to a Gaussian (dotted line) to obtain an estimate for standard deviation of the noise. Higher intensity voxels (inset, 10 × vertical scale) can averaged to estimate the mean signal for the image. The resulting SNR is a convenient statistic for routine comparison of images; calculation is easily automated and less biased than SNR estimates based on regions of interest. (B) Multiecho acquisition scheme for boosting SNR. In this implementation, four echoes refocused by π-pulses are collected per excitation. The pulse sequence (lower part) depicts RF transmit/receive events (labeled RF) and frequency-encoding gradient pulses (G_r; phase and slice-selection gradients not shown). The four blowfly cross sections, numbered 1–4, correspond to signal from four sets of echoes, refocused at echo times of 3, 6, 9, and 12 ms, respectively, in each repetition of the 3D imaging pulse sequence. SNR gains of 30–40% are achieved using this method. Further echo summation is possible but results in limited SNR improvement, due to progressive T_2 relaxation and pulse inhomogeneity across the sample. (C) Test of the stability of fly imaging. Two identical data sets were acquired from the head of a live blowfly, using the experimental parameters given in Fig. 4, but with two transients per echo instead of four (and 9.5 h per acquisition). The panel shows a coronal cross section from the average of the two 3D images (top), compared with an equivalent cross section from a matrix of their variances (bottom). Regions of high variance are mainly peripheral to the optic lobes and brain. The 2D slices shown here roughly correspond anatomically to the view of a separate fly shown in Fig. 4.

images with voxel size $(19.5\,\mu m)^3$, acquired with TR/TE of 500/3 ms and two averages per echo, and filtered only with squared-sinebell apodization, this procedure yielded an average SNR of 9.5 ± 1.3 (mean $\pm$ SD, $n = 6$). This value indicates that intensity differences on the order of 20% at the single-voxel level are reliably discriminable in our highest resolution data sets. The SNR of these images was limited by the need to use strong frequency-encoding gradients to overcome susceptibility gradients in the fly (see above and Fig. 2). With the field of view required to image the fly's head (5 mm) and a read gradient of 59 G/cm, the k-space sampling bandwidth is considerably above the optimum dictated by the fly's mean T_2 relaxation rate of about 20 ms at 14.1 T (data not shown). To partially compensate for this suboptimal bandwidth, we implemented a Carr–Purcell acquisition scheme (Fig. 5B) in which several closely spaced echoes are collected per excitation in the imaging pulse sequence [22]. This method allows effective signal averaging without a concomitant increase in the total measuring time and resulted in gains of 30–40% in SNR.

If the MRI system is used to follow physiological changes as a function of time, the temporal stability of the measurements may be as important a limitation as raw SNR. Sources of confounding instability may range from instrumental fluctuations to motion or metabolic changes in the living specimen. The temporal stability of our 3D images was judged by comparing two $(19.5\,\mu m)^3$-voxel images of the same fly. Fig. 5C shows a coronal cross section taken from the averaged blowfly image, alongside an equivalent cross section of a matrix of intensity variances calculated by voxel between the original two images. Regions of relatively high variance are concentrated in interstitial areas adjacent to but not within the brain and optic lobes; these areas are sites of adipose tissue deposits [24], which were presumably partially depleted over the timespan of our experiments (19 h), during which the fly was not fed. Similar results were obtained with many other specimens under related conditions. As in the vast majority of dozens of 3D fly images we acquired, however, Fig. 5C contains no evidence of gross motion-related distortion; series of 2D images acquired from multiple flies on a faster timescale (minutes per image) also indicated that the specimens were immobile, with the exception of their unrestricted probosces and antennae (data not shown). This demonstrated that our immobilization procedure was successful, although we cannot rule out the possibility that low-amplitude internal motion with even shorter timescale affects the average image intensity.

3.4. Conclusions

We have shown that high-quality 20–40 μm resolution images can be obtained from live blowflies in a 14.1-T MR microscopy system. The images reveal aspects of the fly's neuroanatomy in intricate detail. Although the animals were alive and unanesthetized during experiments, the data are free of movement artifacts and evidence of severe instabilities. Relatively strong gradient pulses (over 50 G/cm) and wide-bandwidth acquisition were required to overcome magnetic susceptibility-induced distortion, but SNR could be recouped by using pulse sequences with echo summation.

These results are offered in large part to demonstrate the utility of the blowfly system as a substrate for future high-resolution MRI investigations of structure and physiology. Because of the robustness of the preparation and the variety of established non-MRI techniques easily brought to bear, the blowfly will be a good testing ground for new MRI methods designed to approach neurophysiology or pathology. Further, because the fly brain can be imaged near cellular resolution—in the sense that signal from individual voxels reflects the structural and physiological parameters of single cells or small groups of cells—subsequent studies with this animal may provide a natural extension for previous work on compartmentalization in single cells, as well as an in vivo context for studies of more complex neuroanatomy. The images we present here also establish a new benchmark in high-resolution noninvasive imaging. Although the voxel dimension and contrast-to-noise are comparable to previously published in vivo images [15], the views of brain structure are unsurpassed in the range 20–40 μm and demonstrate that effective hardware design, specimen preparation, and imaging protocols can overcome the intrinsic challenges to very-high-resolution MR imaging in intact live animals.

Acknowledgments

The authors thank David Cory for advice and access to instrumentation and Markus Meister for important suggestions. We also thank Xiaowu Tang for help with imaging hardware, Rob de Ruyter van Steveninck and Goeff Lewen for tutorials in fly handling, and Don Wiley for initial support and use of laboratory facilities. We are grateful to Zachary Schoening for technical assistance and histology. DOE and NIH grants to David Cory (Dept. of Nuclear Engineering, MIT) provided support for the Bruker AMX II 600 spectrometer. Our work was funded generously by the Whitehead Institute, where A.P.J. is a Whitehead Fellow.

References

[1] X. Zhou, R.L. Magin, J.C. Alameda Jr., H.A. Reynolds, P.C. Lauterbur, Three-dimensional NMR microscopy of rat spleen and liver, Magn. Reson. Med. 30 (1993) 92–97.

[2] P.M. Glover, R.W. Bowtell, G.D. Brown, P. Mansfield, A microscope slide probe for high resolution imaging at 11.7 Tesla, Magn. Reson. Med. 31 (1994) 423–428.
[3] Y. Xia, K.R. Jeffrey, P.T. Callaghan, Purpose-designed probes and their applications for dynamic NMR microscopy in an electromagnet, Magn. Reson. Imaging 10 (1992) 411–426.
[4] E.W. McFarland, A. Mortara, Three-dimensional NMR microscopy: improving SNR with temperature and microcoils, Magn. Reson. Imag. 10 (1992) 279–288.
[5] J.S. Schoeniger, S.J. Blackband, The design and construction of a NMR microscopy probe, J. Magn. Reson. B 104 (1994) 127–134.
[6] S.M. Choi, X. Tang, D.G. Cory, Constant time imaging approaches to NMR microscopy, Int. J. Imaging Systems Technol. 8 (1997) 263.
[7] J.B. Aguayo, S.J. Blackband, J. Schoeniger, M.A. Mattingly, M. Hintermann, Nuclear magnetic resonance imaging of a single cell, Nature 322 (1986) 190–191.
[8] J.S. Schoeniger, N. Aiken, E. Hsu, S.J. Blackband, Relaxation-time and diffusion NMR microscopy of single neurons, J. Magn. Reson. B 103 (1994) 261–273.
[9] P.T. Callaghan, C.J. Clark, L.C. Forde, Use of static and dynamic NMR microscopy to investigate the origins of contrast in images of biological tissues, Biophys. Chem. 50 (1994) 225–235.
[10] S.C. Lee, K. Kim, J. Kim, S. Lee, J. Han Yi, S.W. Kim, K.S. Ha, C. Cheong, One micrometer resolution NMR microscopy, J. Magn. Reson. 150 (2001) 207–213.
[11] R.E. Jacobs, S.E. Fraser, Imaging neuronal development with magnetic resonance imaging (NMR) microscopy, J. Neurosci. Methods 54 (1994) 189–196.
[12] J.F. Kayyem, R.M. Kumar, S.E. Fraser, T.J. Meade, Receptor-targeted co-transport of DNA and magnetic resonance contrast agents, Chem. Biol. 2 (1995) 615–620.
[13] M. Lewin, N. Carlesso, C.H. Tung, X.W. Tang, D. Cory, D.T. Scadden, R. Weissleder, Tat peptide-derivatized magnetic nanoparticles allow in vivo tracking and recovery of progenitor cells, Nature Biotechnol. 18 (2000) 410–414.
[14] R. Weissleder, A. Moore, U. Mahmood, R. Bhorade, H. Benveniste, E.A. Chiocca, J.P. Basilion, In vivo magnetic resonance imaging of transgene expression, Nature Med. 6 (2000) 351–355.
[15] R.E. Jacobs, E.T. Ahrens, T.J. Meade, S.E. Fraser, Looking deeper into vertebrate development, Trends Cell Biol. 9 (1999) 73–76.
[16] M. Egelhaaf, R. Kern, H.G. Krapp, J. Kretzberg, R. Kurtz, A.K. Warzecha, Neural encoding of behaviourally relevant visual-motion information in the fly, Trends Neurosci. 25 (2002) 96–102.
[17] K. Hausen, The lobula-complex of the fly: structure, function and significance in visual behavior, in: M.A. Ali (Ed.), Photoreception and Vision in Invertebrates, Plenum, New York, 1984.
[18] N.J. Strausfeld, Functional Neuroanatomy of the blowfly's visual system, in: M.A. Ali (Ed.), Photoreception and Vision in Invertebrates, Plenum, New York, 1984.
[19] W.E. Conner, G.A. Johnson, G.P. Cofer, K. Dittrich, Magnetic resonance microscopy: in vivo sectioning of a developing insect, Experientia 44 (1988) 11–12.
[20] M. Mapelli, F. Greco, M. Gussoni, R. Consonni, L. Zetta, Application of NMR microscopy to the morphological study of the silkworm, *Bombyx mori*, during its metamorphosis, Magn. Reson. Imaging 15 (1997) 693–700.
[21] S. Wecker, T. Hornschemeyer, M. Hoehn, Investigation of insect morphology by MRI: assessment of spatial and temporal resolution, Magn. Reson. Imaging 20 (2002) 105–111.
[22] P.T. Callaghan, Principles of Nuclear Magnetic Resonance Microscopy, Oxford Univ. Press, Oxford, 1993.
[23] H.G. Krapp, B. Hengstenberg, R. Hengstenberg, Dendritic structure and receptive-field organization of optic flow processing interneurons in the fly, J. Neurophysiol. 79 (1998) 1902–1917.
[24] A. Miller, The internal anatomy and histology of the imago of *Drosophila melanogaster*, in: M. Demerec (Ed.), Biology of drosophila, Facsimile ed., Cold Spring Harbor Laboratory Press, Plainview, NY, 1950.
[25] N.J. Strausfeld, Atlas of an Insect Brain, Springer, New York, 1976.
[26] J.F. McAlpine, Manual of Nearctic Diptera, Agriculture Canada, Ottawa, 1981.